(ISSN: 0973-7049(P))

The Bioscan AN INTERNATIONAL QUARTERLY JOURNAL OF LIFE SCIENCES 21(4): S.I (4),661-675, 2026 www.thebioscan.com

Green Synthesis of Nickel Oxide (NiO) Nanoparticles Using Neem (*Azadirachta indica*) Leaf Extract: Physicochemical Characterization and In Vitro Antidiabetic, Antioxidant, and Antimicrobial Activities

Pujatai A. Nawkhare[1]*, Suresh B. Rewatkar [2]

[1]Dr.Ambedkar College of Arts, Comm. and Science Chandrapur 442401India
[2]Former Dean Science and Technology, Gondwana University Gadchiroli
Corresponding Author : *puja.nawkhare@gmail.com

DOI: https://doi.org/10.63001/tbs.2026.v21.i04.S.I(4).pp661-675

KEYWORDS
Nickel oxide nanoparticles; green synthesis; Azadirachta indica; XRD; FTIR; SEM-EDX; antidiabetic; antioxidant; antimicrobial

Received: 29/09 /2026
Accepted :16/10/2026
Published: 26/10/2026

Abstract
X-ray diffraction (XRD), Fourier transform infrared (FTIR) and scanning electron microscopy (SEM combined with energy dispersive X-ray spectroscopy or EDX) were used to characterize the biosynthesized NiO-Neem nanoparticles using the aqueous leaf extract of neem (*Azadirachta* indica) as a reducing and capping agent. A face centred cubic (bunsenite) NiO lattice with the space group Fm-3m was found to be phase pure, having an average crystallite size of about 6.4 nm (Debye-Scherrer method) and 7.8 nm (Williamson-Hall analysis), and a very small tensile microstrain (~5.1 x 10-4). FTIR spectra indicated the presence of the diagnostic Ni-O stretching doublet near 588 cm-1 and 409 cm-1, and also the presence of bands due to the presence of traces of neem phytoconstituents while SEM-EDX analysis suggested the presence of a surface layer of oxygen with the oxygen to Ni ratio of approximately 2:1, indicating that the Ni metal particles had an oxygen rich surface constitution. In the in vitro bioactivity assays, NiO-Neem nanoparticles were most potent antidiabetic (inhibiting α-glucosidase, IC50 14.51 +/- 0.14 microg/mL and inhibiting about 38-fold better than acarbose) and the most potent antioxidant sample (DPPH radical scavenging ability, IC50 95.24 +/- 0.02 microg/mL). By the agar well diffusion method, organism dependent detection of activity was observed wherein NiO-Neem showed dose dependent activity with a resistance seen for Escherichia coli and Staphylococcus aureus. The present study shows, through the green synthesis using the Plant parts of neem, the synthesis of NiO nanoparticles of uniform size, optimum parameters and optimum concentration of phytochemical coating which exhibited significant biomedical activity (antidiabetic, antioxidant) with desirable organ and application specificity.

1. Introduction

Nanotechnology, which has emerged as one of the most dynamic fields of materials and biomedical science, is well known for its ability to exhibit vastly different physicochemical properties from bulk materials, such as greater surface reactivity, quantum-confinement effects and an extraordinary surface-area-to-volume ratio. Because of their high chemical and thermal stability, catalytic activity, semiconducting properties and compatibility, Nickel oxide (NiO) nanoparticles have been of special interest in the field of biomedical application including gas sensing and storage, antimicrobial agents, antioxidants, enzyme inhibitors, and anti-cancer agents.

The common chemical and physical methods for producing metal-oxide nanoparticles such as co-precipitation, hydrothermal synthesis, sol-gel and physical vapour deposition (PVD) generally use toxic reducing agents or organic solvents/surfactants or high energy input, thus creating concerns about expensive, scalability and environmental and biological safety of the nanoparticles. “Green” synthesis for replacement

of hazardous chemical reductants by plant extracts, microorganisms or other biological agents thus appeared as an attractive alternative, which is low-cost, operationally simple and in addition nanoparticles synthesized in this way have a biocapping on their surface, which has biological activity and other properties that can be added (Abd El-Mageed, T. A 2022).

Azadirachta indica commonly known as Neem is a well studied medicinal plant throughout South Asia and leaves are rich in polyphenols, flavonoids, terpenoids, tannins and other reducing phytoconstituents. Such biomolecules are well characterized to be able to reduce the concentration of the dissolved metal ions from oxides/hydroxides and to adsorb onto the newly formed surface of the nanoparticles as a capping layer which inhibits the growth and agglomeration of the nanoparticles. Previous studies have shown that zinc oxide nanoparticles can be synthesized using neem extract and within 30 min the FTIR and HPLC showed several phenolic fractions on the surface of the nanoparticles and the corresponding antibacterial effect [3-5]. Other extracts derived from 4 different species of leaves, such as Aegle marmelos, Zanthoxylum rhetsa, Areca catechu, and combined species of Medicago, Euphorbia, Codiaeum and Helianthus, have similarly been used to synthesize green NiO nanoparticles that combine antibacterial, antioxidant, and antidiabetic (alpha-amylase/alpha-glucosidase inhibitory) activity, with the magnitude and organism/enzyme selectivity of each activity varying significantly with the plant source employed (Sukumaran, J.,et al., 2025 ., Telagari, M., & Hullatti, K. 2015).

Three of the most prevalent global health burdens are diabetes mellitus, oxidative stress, and microbial infections; and nanomaterials targeting multiple mechanisms are opportunities for particularly translational interest. Pharmacological activity of the inhibitors includes the ability to delay the digestion of carbohydrates and glucose absorption in the intestine (alpha-glucosidase inhibition) and their radical scavenging activities towards the DPPH free radical, which is a widely used benchmark for a compound's ability to neutralise certain reactive oxygen species associated with oxidative-stress-driven disease; and their antibacterial activity against clinically relevant Gram-positive and Gram-negative pathogens was assessed using agar well diffusion assays as a first-pass screen. While there are increasing interest on the green synthesized NiO nanoparticles, there are surprisingly, lower number of reports that include a single set of NiO nanoparticles evaluated simultaneously for detailed structural characterization (XRD, FTIR, SEM, EDX) and for the activity on antidiabetic activities as well as antioxidant and antimicrobial activities against multi-organisms.. To this end, the present work reports physicochemical characterization of NiO nanoparticles (NiO-Neem) obtained using neem leaf extract and their

in vitro alpha-glucosidase inhibitory activity (antidiabetic) and agar well diffusion antimicrobial efficacy in two Gram-negative (Escherichia coli and Pseudomonas aeruginosa) and two Gram-positive (Staphylococcus aureus and Bacillus subtilis) bacteria and evaluate their in vitro antioxidant potential for DPPH radical scavenging .

2. Materials and Methods

2.1 Materials

Fresh leaves of *Azadirachta indica* (neem) were collected locally and used for preparation of the aqueous leaf extract that served as the reducing and capping agent for nanoparticle synthesis.

Nickel nitrate hexahydrate [$Ni(NO_3)_2 \cdot 6H_2O$] (sigmaaddrich), sodium carbonate (Na_2CO_3), 2,2-diphenyl-1-picrylhydrazyl (DPPH), methanol, phosphate buffer, alpha-glucosidase enzyme, acarbose, ascorbic acid, dimethyl sulfoxide (DMSO), Mueller-Hinton broth (MHB), Mueller-Hinton agar (MHA) and ciprofloxacin were of analytical grade and used as received. Whatman No. 1 filter paper was used for filtration, and double-distilled water was used throughout for the preparation of all solutions and extracts.

Four bacterial strains – *Escherichia coli*, *Pseudomonas aeruginosa* (MTCC 3541), *Staphylococcus aureus* (MTCC 96) and *Bacillus subtilis* (MTCC 1133) – were used to evaluate antimicrobial activity.

Instruments and equipment used included a mechanical grinder, magnetic stirrer, centrifuge, hot-air oven and muffle furnace for extract preparation, synthesis and calcination; a powder X-ray diffractometer (Cu Kα radiation) for crystal-structure analysis; a Shimadzu FTIR spectrophotometer (4000–400 cm^{-1}) for surface functional-group analysis; a scanning electron microscope equipped with energy-dispersive X-ray spectroscopy (SEM-EDX) for morphological and elemental analysis; and a microplate reader for the antidiabetic and antioxidant assays. IC50 values were computed using GraphPad Prism 6 software.

2.2 Green synthesis of NiO-Neem nanoparticles

For Neem leaf extract preparation plant material was collected.Plant material was collected for preparation of Neem leaf extract.The shoots of the plant (*Azadirachta indica* - neem) were cut, washed under running tap water, then under running distilled water, to eliminate the loosen dust and believes that the surface dirt. The cleaned leaves were simply cut into small pieces, shade dried and ground them to fine powder in mechanical grinder. The dried powder of leaves was kept for further use in an airtight container at room temperature.

Preparation of the aqueous extract: 10g of neem leaf powder was added to the 200 mL of distilled water in a beaker of glass. It was suspended on a magnetic stirrer for 2 h at 40-60 °C while stirring. Once the mixture had cooled down to room temperature it was left to macerate over night. The extract was then passed through Whatman No.1 filter paper and centrifuged for 15 minutes at 2000 rpm to prevent the fine particulates from going through. The supernatant liquid was

filtered and stored at 4 °C temperature for making nanoparticles. The colour of the obtained neem leaf extract was light brown.

The solution preparation is in the process.The preparation of the nickel precursor solution is in progress.

Nickel nitrate hexahydrate [$Ni(NO_3)_2 \cdot 6H_2O$] was dissolved in distilled water to form a 0.02 M solution. The mass of $Ni(NO_3)_2 \cdot 6H_2O$ that would be required to prepare a 1000 mL solution of 0.02 M is calculated as follows:

$$\text{mass} = M \times V \times \text{MW}$$
$$= 0.02 \text{ mol L}^{-1} \times 1 \text{ L}$$
$$\times 290.8 \text{ g mol}^{-1} \approx 5.82 \text{ g}$$

Approximately 5.82 g of $Ni(NO_3)_2 \cdot 6H_2O$ was dissolved in distilled water and diluted to 1000 mL. The resulting precursor solution exhibited a characteristic green color due to the presence of Ni^{2+} ions.

Green synthesis of nickel oxide nanoparticles using Neem extract

In a typical synthesis, 1000 mL of 0.02 M $Ni(NO_3)_2 \cdot 6H_2O$ solution was taken in a 1000 mL beaker. To this, 200 mL of neem leaf extract was added slowly under continuous stirring. The reaction mixture was maintained at 50–60 °C and stirred at 1000 rpm for 3 h; phytochemicals present in the neem extract (e.g., polyphenols, flavonoids, and terpenoids) acted as both reducing and capping agents, facilitating the formation and stabilization of nickel oxide precursor nanoparticles.

During the reaction, a color change from light green to blue-green was observed, indicating the formation of NiO precursor nanoparticles. The mixture was then centrifuged at 10,000–20,000 rpm for 15 min to collect the precipitate. The pellet was filtered through Whatman No. 1 filter paper and washed repeatedly with distilled water to remove unreacted ions and residual plant metabolites. The washed precipitate was dried in an oven at 80 °C to obtain a dry powder of NiO precursor/nanoparticles.

Calcination

The dried powder was calcined in a muffle furnace at 400 °C for 1–2 h to convert nickel hydroxide/organic–metal complexes into crystalline nickel oxide (NiO) nanoparticles. Calcination at 400 °C is commonly reported to yield cubic NiO with improved crystallinity and well-defined nanoparticle morphology.

2.3 Physicochemical characterization

The crystal structure and phase purity of NiO-Neem nanoparticles was investigated by powder XRD with Cu Kalpha radiation (lambda = 1.54059 A) in the diffraction range corresponding to the (111), (200), (220), (311) and (222) reflections of NiO cubic structure. The diffraction peaks were translated using ICDD reference card 01-010-0095. The cubic lattice parameter was calculated for each diffraction peak d = a / (sqrt(h^2+k^2+l^2)), where a is the lattice parameter. Crystallite size was estimated from the Debye-Scherrer equation (D = K.lambda / (beta.cos(theta))) and by Williamson Hall analysis (beta.cos(theta) = K.lambda/D + 4.epsilon.sin(theta)), where K = 0.9 is a constant and lambda is the X-ray wavelength. FTIR spectroscopy (Shimadzu FTIR spectrophotometer 4000-400cm-1) has been used to identify the surface functional groups. The surface morphology was analysed using scanning electron microscopy (SEM) at magnifications ranging from 100x to 50000x and elemental composition was analysed by energy-dispersive X-ray spectroscopy (EDX, eZAF quantification) at an accelerating voltage of 10 kV.

2.4 Antidiabetic activity (alpha-glucosidase inhibition assay) in vitro.

Alpha Glucosidase inhibition assay [9] was used to assess the antidiabetic potential. A reaction mixture containing corresponding amounts of

phosphate buffer (100 mM, pH 6.8), alpha-glucosidase enzyme (1 U/mL) and varied amounts of each nordapatide sample (1-1000 microg/mL) was incubated for 15 min at 37° C and Na2CO3 (0.1 M) was thereafter added to terminate the reaction. A microplate reader set at 405 nm was used to measure the absorbance of the free p-nitrophenol. Acarbose was used as a positive control. The percentage inhibition was computed as %Inhibition = [(A(control) - A(test))/A(control)] x 100 and IC50 values determined from dose response curve using GraphPad Prism 6.

2.5 In vitro antioxidant activity (DPPH radical scavenging activity)

The free-radical scavenging activity was evaluated with the DPPH assay which employs the antioxidant 2,2-diphenyl-1-picrylhydrazyl (DPPH). 10 microL of test compound at different concentrations (1 microg/mL – 1000 microg/mL) was mixed with 0.2 mL of 0.1 mM DPPH in methanol in a 96-well plate. The positive standard was ascorbic acid. Reactions were conducted in quadruplicate and on duplicate blanks (DPPH-free) and replicates with no DPPH on each concentration series were incubated in the dark for 30 min and absorbance at 517 nm was measured using a microplate reader . The radical-scavenging action was calculated as %RSA = [Abs (control - sample) / Abs (control)] x 100, and IC50 values for these tests obtained from plots of % inhibition per concentration according to the correlation software GraphPad Prism 6.

2.6 Antimicrobial activity (agar well diffusion assay)

The following pathogens were selected Escherichia coli, Pseudomonas aeruginosa (MTCC 3541), Staphylococcus aureus (MTCC 96) and Bacillus subtilis (MTCC 1133). For the determination of antibacterial activity, the agar well diffusion (Kirby-Bauer based) method was used as described by the American Society for Microbiology Kirby-Bauer Well Diffusion Susceptibility Test Protocol. Bacterial suspensions with turbidity standard of 0.5 McFarland (equal to ~1.5 x 10^8 colony forming units (CFU)/mL) in Mueller-Hinton broth (MHB) were spread on Mueller-Hinton agar (MHA) plates (100 microL). Each of the nanoparticle samples (50 microL) was given a series of dilutions ranging from 0 (DMSO vehicle control) to 312.5 to 625 to 1250 to 2500 to 5000 microg/well against E. coli, P. aeruginosa and S. aureus, and 0-10000 microg/well against B. subtilis. Positive control was given as Ciprofloxacin at concentration of 3 microg/well. Plates were cultivated at 37 degC for 24 h in triplicates (A, B, C) and the clear area of inhibition around each well was measured in mm (Christenson, J. C 2008).

3. Results and Discussion

3.1 XRD analysis: phase identification and crystallite size

The XRD pattern of NiO-Neem (Figure 1) showed five well-resolved reflections at 2theta ~ 37.02, 43.09, 62.81, 75.38, and 79.39 degrees, indexed to the (111), (200), (220), (311), and (222) planes of face-centred cubic (bunsenite) NiO, space group Fm-3m (ICDD 01-010-0095), superimposed on a broad, noisy background between ~10-35 degrees attributable to residual amorphous/organic phytoconstituents from the neem extract. The (200) reflection was the most intense peak, consistent with the standard NiO powder diffraction pattern. No reflections corresponding to Ni(OH)2, metallic Ni, or other secondary/impurity phases were detected, confirming phase-pure crystalline NiO.

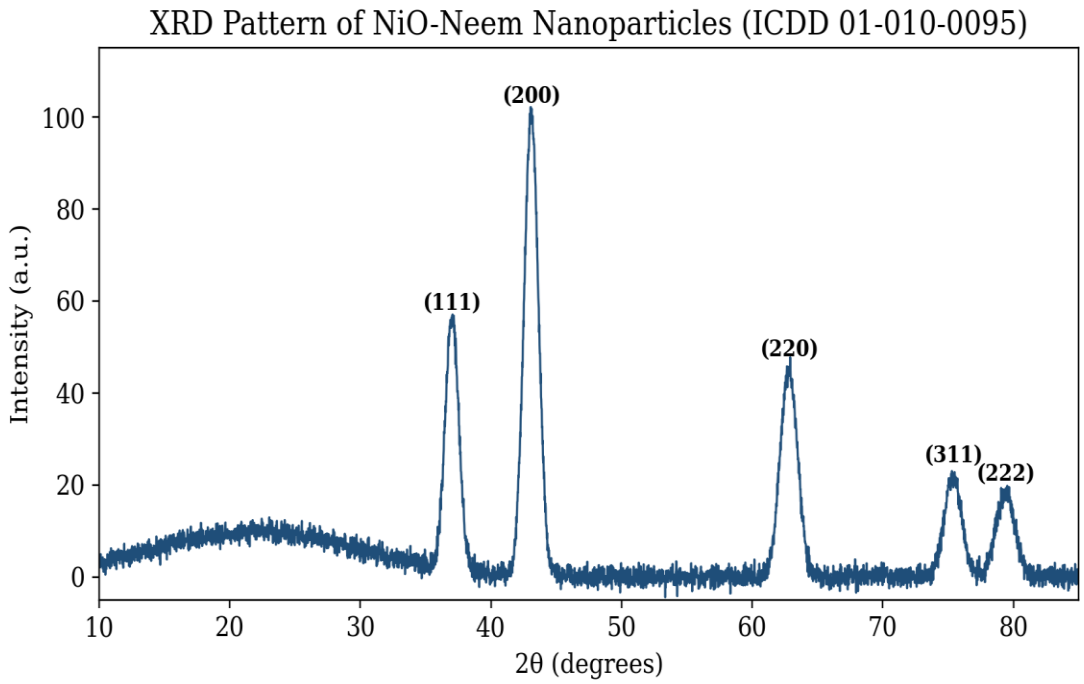


Figure 1. XRD pattern of NiO-Neem nanoparticles, indexed to the (111), (200), (220), (311), and (222) reflections of cubic NiO (ICDD 01-010-0095). Pattern reconstructed from the peak positions, relative intensities, and FWHM values reported in this study (Table 1).

2θ (deg)	d-spacing (Å)	(hkl)	FWHM (deg)	Relative intensity	a (Å)	D (nm)
37.02	2.4265	(111)	1.21	Medium	4.2028	6.92
43.09	2.0976	(200)	1.292	Strongest	4.1952	6.61
62.81	1.4784	(220)	1.56	Medium	4.1815	5.97
75.38	1.2599	(311)	1.56	Weak	4.1786	6.44
79.39	1.2060	(222)	1.75	Weak	4.1777	5.90

Table 1. Indexed XRD reflections, lattice parameter (a), and Scherrer crystallite size (D) for NiO-Neem nanoparticles. Source: XRD characterization data (this study).

The average lattice parameter, calculated from all five reflections, was a = 4.187 +/- 0.010 A, in close agreement with the standard value for cubic NiO (a = 4.176-4.180 A); the slight (~0.2%) expansion is commonly reported for green-synthesized NiO and attributed to lattice strain/surface defects introduced by capping biomolecules. Crystallite size estimated by the Debye-Scherrer equation averaged D ~ 6.4 +/- 0.4 nm, consistent with the instrument software's own reported values (6.2-7.2 nm).

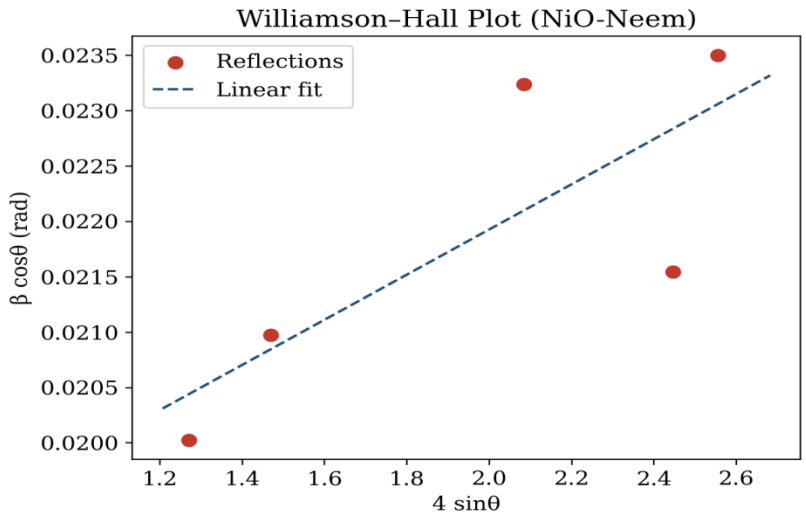


Figure 2. Williamson-Hall plot (beta cos(theta) vs. 4 sin(theta)) for NiO-Neem nanoparticles, separating crystallite-size and microstrain contributions to peak broadening. Source: plotted from the XRD reflection data reported in this study (Table 1).

The Williamson-Hall analysis revealed even smaller crystallite size (D ~ 7.8 nm) as well as small tensile microstrain (epsilon ~ 5.1 x 10-4; dislocation density delta ~ 2.5 x 10^16 lines/m2). The higher W-H estimate compared to the pure-Scherrer average has resulted from small crystallite size, and is accompanied by a small but appreciable broadening as a result of strain - an element typical of biosynthesized metal-oxide nanoparticles, where the small size of the crystallite is accompanied by a mild lattice strain brought about by plant phytochemicals (Kale *et al*., 2026).

3.2 The functional groups, phytochemical capping

The FTIR spectrum of NiO-Neem (Fig.3) had a strong, well defined pair of bands, ranging in wavenumbers from 588.31 to 408.93 cm-1 which are associated with NiO stretching vibration and are broadly reported as diagnostic fingerprint of cubic NiO. A single broad band was assigned to the O-H stretching of moisture and hydroxyl-containing biomolecules adsorbed on the surface of the nanoparticles, which originated from other mid-infrared bands ranging from 935 to 1636 cm-1) assigned to the phytoconstituents, such as phenolics, flavonoids and terpenoids, that were remaining on the surface of the nanotechnology particles.

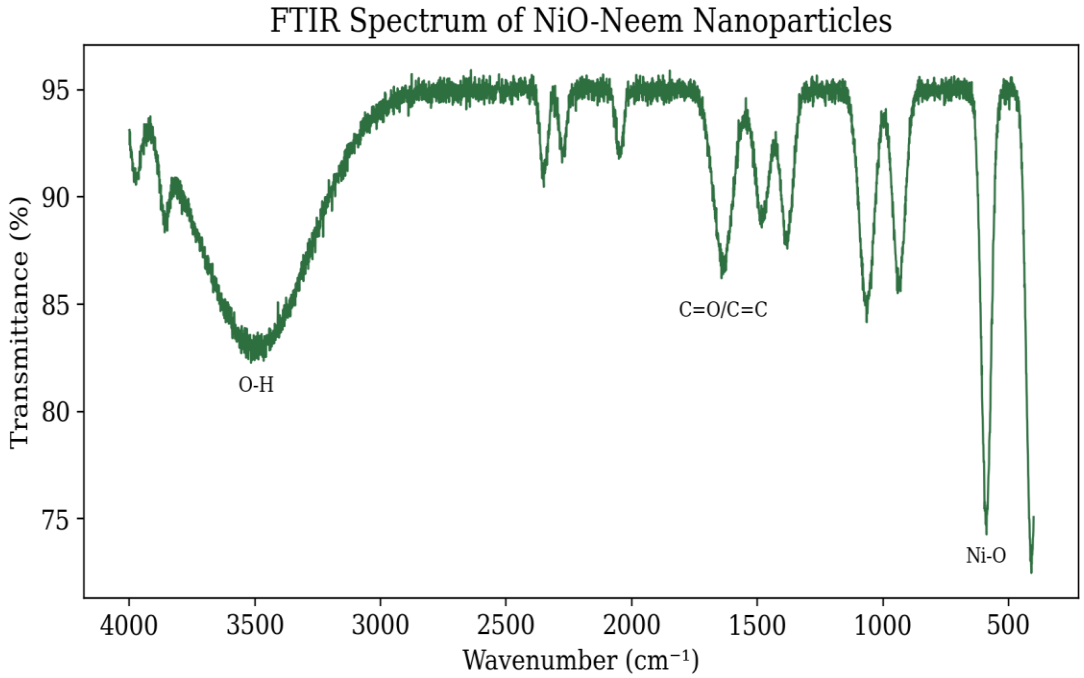


Figure 3. FTIR spectrum of NiO-Neem nanoparticles (4000-400 cm-1), reconstructed from the peak positions reported in this study (Table 2); the Ni-O, C=O/C=C, and O-H regions are labelled.

Peak (cm⁻¹)	Assignment	Interpretation
408.93, 588.31	Ni-O stretching	Fingerprint of NiO lattice formation
935.52	C-O/C-H bending	Phenolic/aromatic groups from neem extract
1063.79	C-O stretching	Flavonoid/terpenoid sugars coating surface
1382.06	C-N / O-H bending	Amine/carboxylate groups of plant biomolecules
1480.43	C=C aromatic stretching	Phenolic (flavonoid) ring vibrations
1635.71	C=O / C=C stretching	Protein/flavonoid reducing agents
3494.20	O-H stretching (broad)	Surface-adsorbed water/hydroxyls

Table 2. Selected FTIR peak assignments for NiO-Neem nanoparticles. Source: FTIR characterization data (this study).

The absence of a sharp, intense nitrate-associated band near 1384 cm-1 (expected for an uncalcined nickel nitrate/hydroxide precursor) indicates that calcination at 400 degC effectively decomposed residual nitrate and organometallic complexes, consistent with the formation of phase-pure crystalline NiO. Together, the FTIR data support a dual role for neem phytochemicals as reducing and capping agents during synthesis, in agreement with comparable neem- and other plant-extract-mediated syntheses of metal-oxide nanoparticles in which phenolic and flavonoid bands are similarly retained on the nanoparticle surface (El-Beltagi, H. S *et al*., 2024., Mankad *et al*.,2016)

3.3 SEM-EDX analysis: morphology and elemental composition

The NiO—A. Neem particles were observed by SEM and at low magnification (100×; Figure 4a) were found to be agglomerates with irregular shape and up to several tens of μ size, which is typical for a powder of particles pyrolysized using a green synthesis method, after drying/calcination where the van der Waals forces and the possibility of biomolecules to

remain in the powder can lead to particle agglomeration. At higher magnifications (50,000x) the internal structure of those larger micron-sized aggregations can be resolved as many smaller, quasi-spherical primary particles closely clustered together, with some inter-particle porosity and fissures visible during drying/calcination (Figure 4b). The quasi spherical NiO nanoparticles had the average size as less than 100 nm as minimum, which matched the results obtained from the NiO nanoparticles by the process of successful nanoscale reduction of NiO nanoparticles by applying the natural routes such as the neem leaf extract.

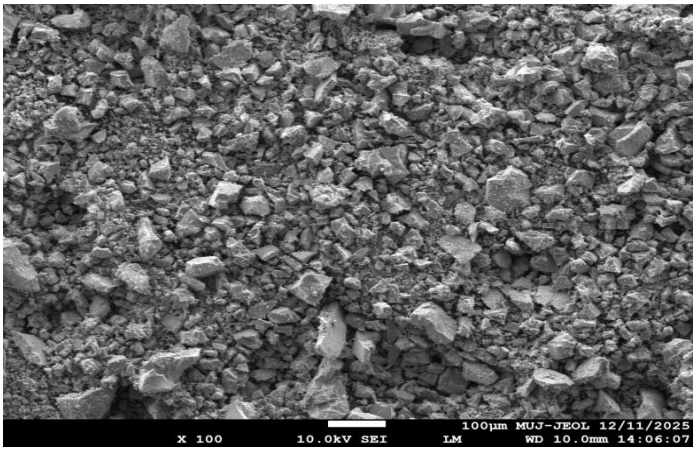


Figure 4a. SEM micrograph of NiO-Neem powder at 100x magnification (scale bar = 100 µm), showing bulk agglomerate morphology. Source: SEM-EDX characterization data (this study).

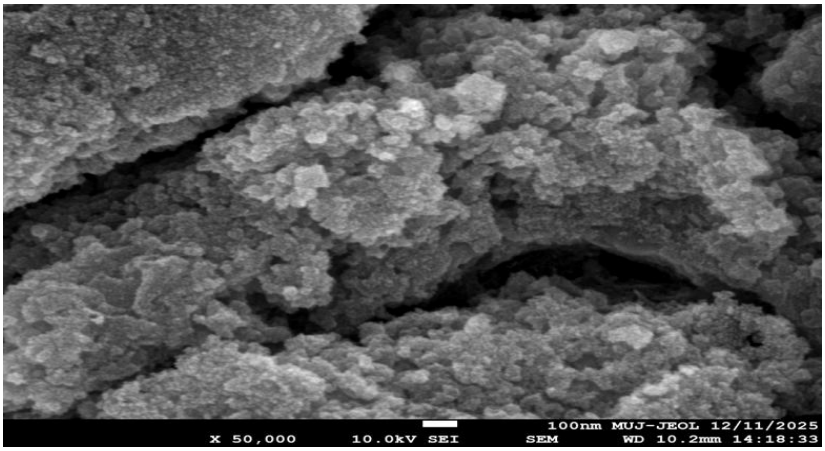


Figure 4b. SEM micrograph at 50,000x (scale bar = 100 nm), showing individual primary nanoparticle boundaries. Source: SEM-EDX characterization data (this study).

EDX analysis (sum spectrum, 10 kV, 6500x, 128.9 s live time) showed only two dominant peaks, corresponding to oxygen (O K) and nickel (Ni L), with no additional peaks attributable to impurity elements, confirming the absence of detectable contamination from precursor salts or synthesis by-products. Quantitative eZAF analysis yielded a composition of 35.6 wt% (67.0 at%) oxygen and 64.4 wt% (33.0 at%) nickel (Table 3) - an O:Ni atomic ratio of approximately 2:1 that deviates from the stoichiometric 1:1 ratio of bulk NiO. This oxygen enrichment is commonly reported for green-synthesized metal-oxide nanoparticles and is attributed to surface-adsorbed hydroxyl groups, residual oxygenated phytochemicals capping the nanoparticle surface,

and the high surface-area-to-volume ratio of nanoscale particles favouring additional oxygen chemisorption [6].

Element	Weight %	Atomic %	Error %
O K	35.6	67.0	7.3
Ni L	64.4	33.0	8.0

Table 3. eZAF quantitative EDX results for NiO-Neem nanoparticles. Source: SEM-EDX characterization data (this study).

3.4 In vitro antidiabetic activity

Dose-dependent inhibition of alpha-glucosidase was observed for all nanoparticle samples tested. Acarbose (positive control) inhibited the enzyme by up to 61.49% at 1000 microg/mL, giving an IC50 of 551.1 +/- 0.03 microg/mL. NiO-Neem nanoparticles showed markedly stronger inhibitory activity, reaching 28.23% inhibition at only 1 microg/mL and 98.84% at 1000 microg/mL (Figure 5), with a calculated IC50 of 14.51 +/- 0.14 microg/mL - approximately 38-fold more potent than acarbose.

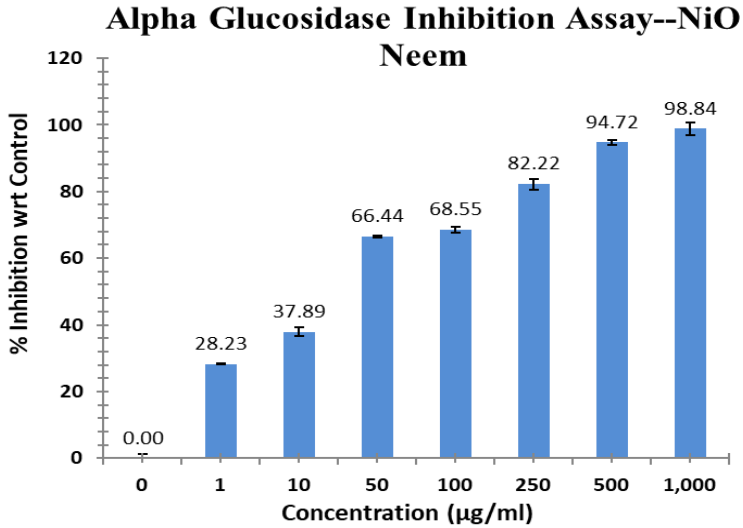


Figure 5. Alpha-glucosidase inhibition (%) versus concentration for NiO-Neem nanoparticles. Source: alpha-glucosidase inhibition assay data

Sample	IC50 (µg/mL, mean ± SEM)
Acarbose (standard)	551.1 ± 0.03
NiO-Neem	14.51 ± 0.14

Table 4. IC50 values (alpha-glucosidase inhibition assay) for NiO-Neem and reference samples. Source: alpha-glucosidase inhibition assay data.

NiO-Neem formulation was highly effective as compared to other three NiO formulations with IC50 value of 14.51 +/- 0.14 microg/mL. Both the surface activity and the uniform small primary particle size observed by SEM (Section 3.3) that would enhance the available surface area of enzyme interacting sites as well as the oxygen-rich phytochemical capped surface crucially indicated by EDX and FTIR would define the enhanced activity of this surface chemistry (structure-activity) relationship also in the case of other plant mediated NiO and metal-oxide nanoparticle systems investigated for alpha-

amylase/alpha-glucosidase inhibition (Said, A. H et al., 2025 ., Loyola-Leyva, A *et al*., 2025).

3.6 In vivo antioxidant activity

The ascorbic acid (positive control) exhibited a typical dose-dependent scavenging activity with IC50 of 19.97 +/- 0.02 microg/mL with the highest inhibition of 84.20% at 50 microg/mL and the lowest inhibition of 0.85% at the lowest concentration (0.78 microg/mL). In terms of antioxidant activity, NiO-Neem showed the highest inhibition starting from 3.02% at the lowest dosage of 1 microg/mL till the highest one at 1000 microg/mL concentration of 90.53% (Figure 6) and IC50 of 95.24 +/- 0.02 microg/mL.

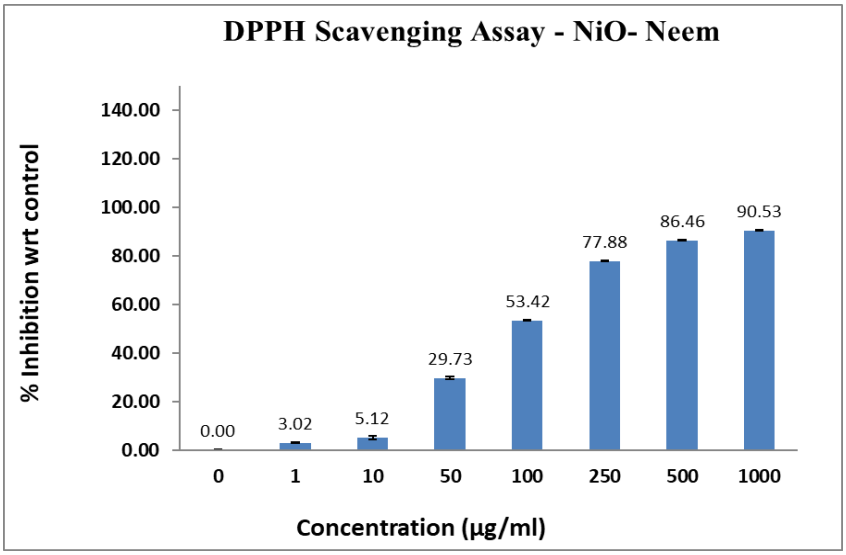


Figure 6. DPPH radical scavenging activity (%) versus concentration for NiO-Neem nanoparticles. Source: DPPH radical scavenging assay data (this study).

NiO-Neem outperformed. This antioxidant potency parallels the antidiabetic result (Section 3.4) and supports the interpretation that the neem-derived phytochemical coating identified by FTIR (phenolics, flavonoids) confers genuine free-radical-scavenging capacity on the NiO-Neem surface, consistent with reports that neem-extract-capped nanoparticles retain multiple bioactive phenolic fractions (El-Beltagi et al., 2024, Abubakar, A et al., 2020., Imam, M. Z., 2011)

3.6 **Antimicrobial activity**

Agar well diffusion assays against four bacterial species revealed clearly organism-dependent antibacterial activity for NiO-Neem (Table 5, Figure 7).

Organism (Gram type)	NiO-Neem activity	Positive control (ciprofloxacin) zone
E. coli (Gram-negative)	5 mm at 312.5 µg (weak/negligible)	31 mm
P. aeruginosa (Gram-negative)	Dose-dependent; 0 mm up to 625 µg, rising to 15.33 ± 1.15 mm at 5000 µg	28 mm
S. aureus (Gram-positive)	No zone at any concentration up to 5000 µg	22.33 ± 5.51 mm
B. subtilis (Gram-positive)	0 mm up to 5000 µg; threshold zone of 12 ± 0 mm at 10000 µg	26 mm

Table 5. Summary of NiO-Neem antibacterial activity (agar well diffusion) against four bacterial species. Source: Aakaar Biotechnologies Pvt. Ltd. contract testing reports (Sample Refs. 25F62E, 25F62G, 25F62H, and companion E. coli report)

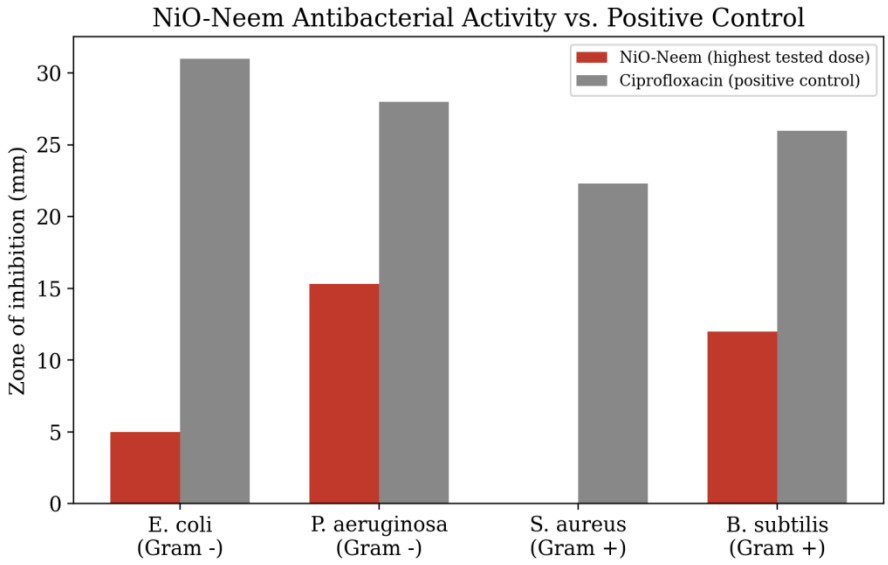


Figure 7. NiO-Neem zone of inhibition (highest tested dose) compared with the ciprofloxacin positive control across all four organisms tested. Source: plotted from agar well-diffusion assay data reported in this study (Table 5).

Against P. aeruginosa, NiO-Neem showed a clear, monotonic, concentration-dependent increase in zone diameter from 1250 to 5000 microg/well (Figure 8), reaching about 55% of the ciprofloxacin zone at the highest dose - a low-to-moderate sensitivity response by conventional well-diffusion classification. No inhibition was recorded at 0, 312.5, or 625 microg/well.

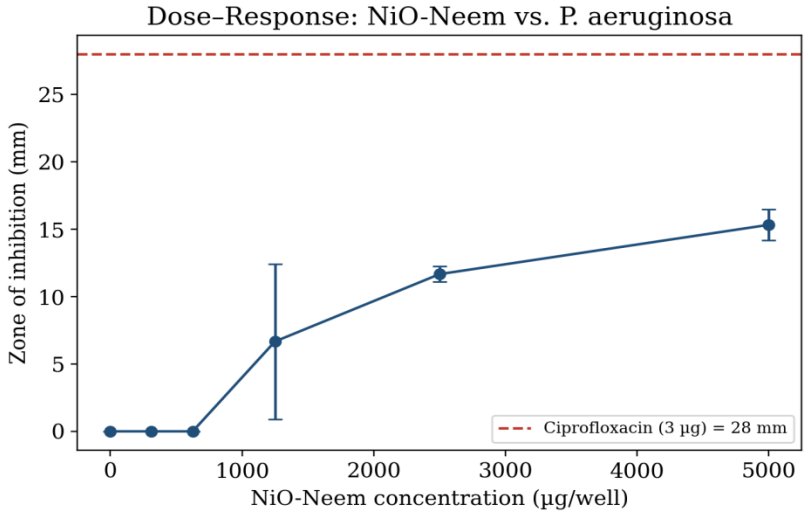


Figure 8. Dose-response curve for NiO-Neem nanoparticles against P. aeruginosa (mean ± SD, n = 3), with the ciprofloxacin positive-control zone shown as a reference line. Source: plotted from agar well-diffusion assay data reported in this study.

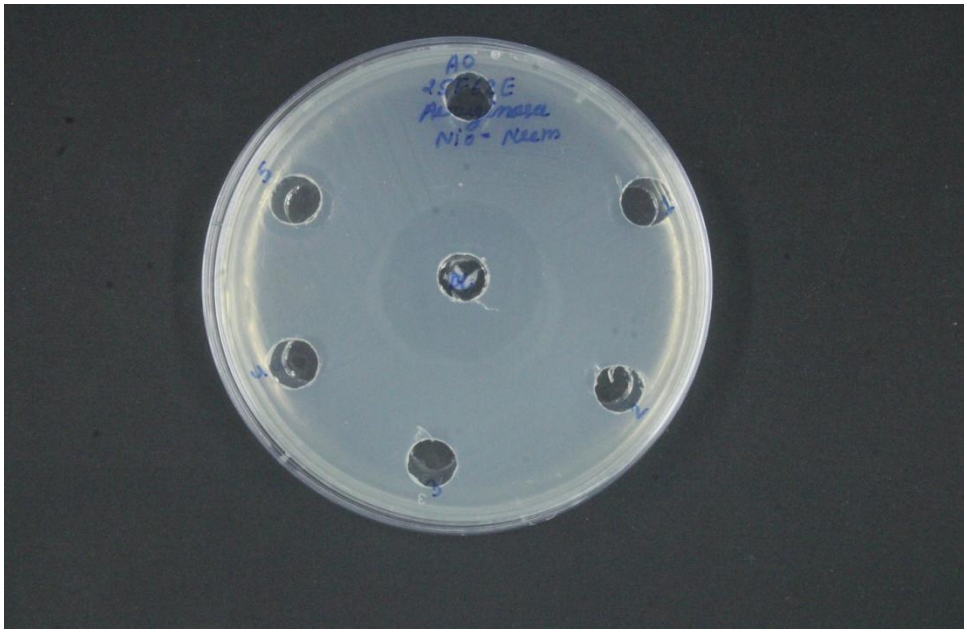


Figure 9. Representative agar well-diffusion plate for NiO-Neem against P. aeruginosa. Centre well = ciprofloxacin positive control; peripheral wells = NiO-Neem dilutions. Source: Aakaar Biotechnologies Pvt. Ltd., contract testing report, Sample Ref. 25F62E (this study).

Against the Gram-positive B. subtilis, NiO-Neem was one of only two of nine tested samples to show any measurable activity, producing a reproducible 12 mm zone at the highest tested concentration (10000 microg/well; Figure 10), while no zone was observed at or below 5000 microg/well.

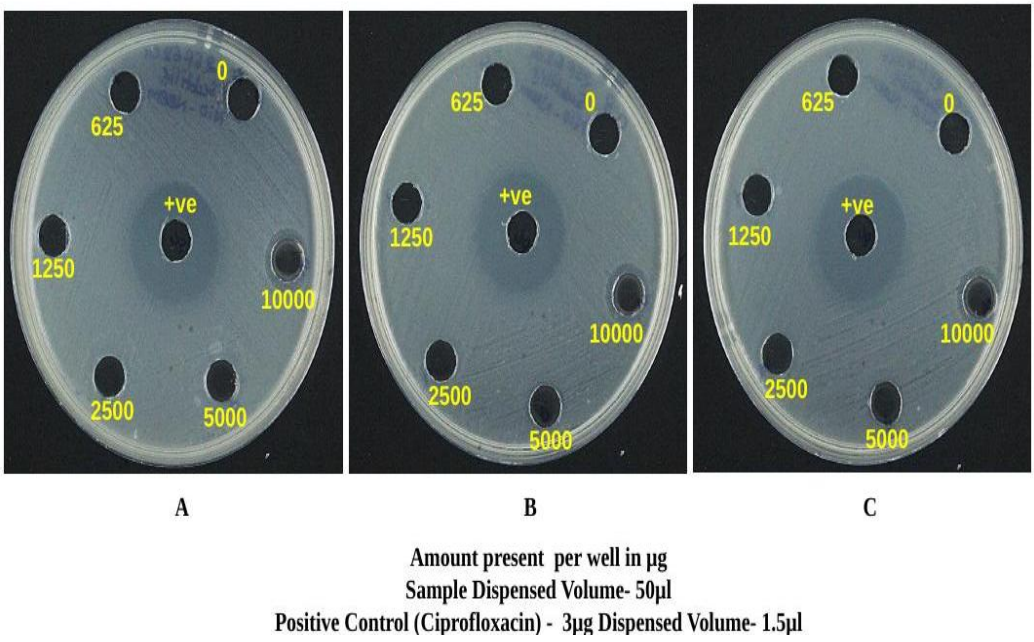


Figure 10. Triplicate agar well-diffusion plates (A, B, C) for NiO-Neem against B. subtilis, showing a visible zone around the 10000 µg well and the central ciprofloxacin positive control. Source: Aakaar Biotechnologies Pvt. Ltd., contract testing report, Sample Ref. 25F62G (this study).

NiO-Neem, however, had minimal inhibition with E coli (5 mm at 312.5 microg/well, one of the nine least inhibitory), and was completely inactive against S. aureus in all of the 10 concentrations tested up to 5000 microg/well, with a good response obtained by ciprofloxacin (positive control). The pattern (registered antibacterial activity against P. aeruginosa and B. subtilis, but not against other Gram-negative and Gram-positive representatives of the same group E. coli and S. aureus) shows that the antibacterial effect of NiO-Neem nanoparticles is not just Gram-type dependent, but species dependent. Similar organismspecific activity has also been observed for other plant NiO NP systems which showed that the plant source and the corresponding surface phytochemistry also influenced the species-specific susceptibility to antibacterial activity, apart from the overall Gram-positive/Gram-negative effect (Kale *et al.,* 2026, Loyoloa –Leyva A *et al.,* 2025).Reactive-oxidation-species generation, release of Ni2+ ions and direct disruption of the membrane/cell wall are plausible mechanisms responsible for the observed pattern, and scale with the dose of nanoparticles and surface area loading, with species-specific differences in the outer-membrane permeability, efflux-pump activity and structure of peptidoglycan/wall-teichoic-acid as a modifying factor.

When combined with its consistently high, antidiabetic, and antioxidant activity (Sections 3.4–3.5), NiO-Neem seems to be a nanoparticle system with primary biomedical applications involving enzyme inhibition and scavenging of free radicals, but with some restricted specific applications that are just limited to pantheon of microorganisms such as B. subtilis- and P. aeruginosa-type species.

4. Conclusion

The green synthesis of phase-pure NiO nanoparticles with an average crystallite size of ~6-8 nm was successfully mediated using neem leaf extract, which was confirmed by XRD, and supported by FTIR and SEM-EDX, where the phytochemical-capped NiO fraction was revealed as an oxygen-rich, sub-100 nm particulate surface. NiO-Neem nanoparticles exhibited an extremely high in vitro antidiabetic activity (alpha-glucosidase IC50 =14.51 microg/mL) compared to other nine samples of related metal-oxide nanoparticles and plant extracts which were investigated and exhibited comparatively low activity, with the highest recorded activity being for the NiO derivative, more than 38 folds higher than the standard antidiabetic drug, control acarbose, and the strongest antioxidant activity (DPPH IC50 = 95.24 microg/mL) of the said 9 sample panel, with comparatively low activity observed against Antimicrobial agents such as P. aeruginosa and B. subtilis. The synthesized NiO-Neem nanoparticles are a promising low-cost, environment friendly material for biomedical applications in antidiabetic and antioxidant field, which need to be further explored by performing some kinetic (such as Lineweaver-Burk) studies, in vivo and in vitro studies and structure-activity relationship studies to elucidate their structure and translation.

References

[1] Said, A. H., Shaibah, F., Moustafa, M., & Elamary, R. B. (2025). Plant-mediated nickel oxide nanoparticles show species-dependent

antibacterial, antioxidant, anti-inflammatory and antidiabetic activities. Scientific Reports, 15, Article 31096.

[2] Abd El-Mageed, T. A., Abdelbaky, A. S., Babalghith, A. O., Selim, S., & Mohamed, A. M. H. A. (2022). Green synthesis and characterization of ZnO nanoparticles using Pelargonium odoratissimum (L.) aqueous leaf extract and their antioxidant, antibacterial and anti-inflammatory activities. Antioxidants, 11(8), 1444.

[3] El-Beltagi, H. S., Ragab, M., Osman, A., El-Masry, R. A., Alwutayd, K. M., Althagafi, H., Alqahtani, L. S., Alazragi, R. S., Alhajri, A. S., & El-Saber, M. M. (2024). Biosynthesis of zinc oxide nanoparticles via neem extract and their anticancer and antibacterial activities. PeerJ, 12, e17588.

[4] Tsegahun, E., & Aklilu, M. (2025). Neem (Azadirachta indica) leaf extract mediated synthesis of zinc oxide nanoparticles (ZnO NPs) and their antibacterial activity. Discover Nano, 20(1), 145.

[5] Mankad, M., Patil, G., Patel, S., Patel, D., & Patel, A. (2016). Green synthesis of zinc oxide nanoparticles using Azadirachta indica A. Juss. leaves extract and its antibacterial activity against Xanthomonas oryzae pv. oryzae. Annals of Phytomedicine, 5, 76–86.

[6] Sukumaran, J., Priya, M., Venkatesan, R., Sathiasivan, K., Khan, M. R., & Kim, S.-C. (2025). Green synthesis of nickel oxide nanoparticles using leaf extract of Aegle marmelos and their antibacterial, anti-oxidant, and in vitro cytotoxicity activity. Microscopy Research and Technique, 88(11), 2830–2842.

[7] Kale, S. S., Nikum, A. P., Pawar, Y. A., Gurav, V. L., & Sathe, G. B. (2026). Green synthesis of nickel oxide nanoparticles using Zanthoxylum rhetsa (Roxb.) DC. leaf extract, comprehensive physicochemical characterisation and multifunctional biomedical applications. Discover Green Chemistry, 1, Article 15.

[8] Loyola-Leyva, A., Hernandez-Vidales, K., Ruiz-Garcia, J., & Loyola-Rodriguez, J. P. (2025). Characterization of green synthesized nanoparticles with anti-diabetic properties: A systematic review. Current Diabetes Reviews, 21(7), 67–85.

[9] Telagari, M., & Hullatti, K. (2015). In-vitro alpha-amylase and alpha-glucosidase inhibitory activity of Adiantum caudatum Linn. and Celosia argentea Linn. extracts and fractions. Indian Journal of Pharmacology, 47(4), 425.

[10] Christenson, J. C., Korgenski, E. K., & Relich, R. F. (2018). Laboratory diagnosis of infection due to bacteria, fungi, parasites, and rickettsiae. In S. S. Long, C. G. Prober, & M. Fischer (Eds.), Principles and Practice of Pediatric Infectious Diseases (5th ed., pp. 1447–1459.e4). Elsevier.

[11] Abubakar, A., Olorunkemi, M. R., Busari, M. B., Hamzah, R. U., & Abdulrasheed-Adeleke, T. (2020). Comparative in vitro antioxidant activities of aqueous extracts of Garcinia kola and Buchholzia coriacea seeds. Tanzania Journal of Science, 46(2), 498–507.

[12] Imam, M. Z., Akter, S., Hoque Mazumder, M. E., & Rana, S. (2011). Antioxidant activities of different parts of Musa sapientum L. ssp. sylvestris fruit. Journal of Applied Pharmaceutical Science, 1(10), 68–72.

[13] Kirby-Bauer Well Diffusion Susceptibility Test Protocol. American Society for Microbiology (ASM).